Geophysical Research Letters

RESEARCH LETTER
10.1029/2023GL103840

Offshore Migration of Summer Monsoon Low-Level Jet on a Diurnal Scale

Y. Du[1,2,3]

[1]School of Atmospheric Sciences, Sun Yat-sen University, and Southern Marine Science and Engineering Guangdong Laboratory (Zhuhai), Zhuhai, China, [2]Guangdong Province Key Laboratory for Climate Change and Natural Disaster Studies, Sun Yat-sen University, Zhuhai, China, [3]Key Laboratory of Tropical Atmosphere-Ocean System (Sun Yat-sen University), Ministry of Education, Zhuhai, China

Key Points:

- The monsoon low-level jet migrates eastward from the eastern offshore of India at midnight to the center of the Bay of Bengal by afternoon
- The offshore diurnal migration is driven by inertia-gravity waves resulting from the diurnal thermal contrast between land and sea
- The westerly upstream wind from the Indian subcontinent extends the offshore migration, rather than confining it to the coast

Supporting Information:

Supporting Information may be found in the online version of this article.

Correspondence to:

Y. Du,
duyu7@mail.sysu.edu.cn

Citation:

Du, Y. (2023). Offshore migration of summer monsoon low-level jet on a diurnal scale. *Geophysical Research Letters*, *50*, e2023GL103840. https://doi.org/10.1029/2023GL103840

Received 27 MAR 2023
Accepted 29 SEP 2023

Abstract This study investigates the diurnal migration of the low-level jet (LLJ) over the Bay of Bengal in the summer monsoon, which remains understudied despite the well-documented diurnal offshore propagation of rainfall worldwide. The southwesterly LLJ exhibits maximum strength during the night and morning. The LLJ undergoes a substantial eastward migration of approximately 600 km from the eastern offshore of India at midnight to the center of the Bay of Bengal by afternoon. A linear land-sea breeze model is effective in capturing the diurnal migration with similar speed and phase. Including background wind offshore extends the migration, rather than confining it to the coast. This migration is driven by inertia-gravity waves arising from the diurnal land-sea thermal contrast and is influenced by the westerly upstream wind from the Indian subcontinent. Our results have important implications for understanding diurnal monsoon circulations and their associated precipitation.

Plain Language Summary The low-level jet (LLJ) in the summer monsoon plays a crucial role in affecting nocturnal downstream precipitation in South Asia. Previous studies have primarily concentrated on changes in the jet's strength during the day, neglecting its varying location. The present study addresses this gap by providing a comprehensive examination of the previously neglected aspect of the diurnal offshore migration of the LLJ over the Bay of Bengal. The diurnal migration is driven by the difference in temperature between the land and sea and is also aided by upstream wind, in a manner similar to the diurnal offshore propagation of rainfall. Overall, this study offers a more complete understanding of the LLJ' behaviors in the summer monsoon, which can help explain how it affects rainfall in the region.

1. Introduction

Diurnal variation in rainfall and wind is a widespread and well-documented phenomenon that is primarily driven by solar radiation. Typically, rainfall reaches its maximum in the afternoon on land and at night over the ocean (Johnson, 2011). Coastal regions experience alternating sea breeze and land breeze that also exhibit diurnal variation (Rotunno, 1983). Intense low-level winds near coasts, known as coastal low-level jets (LLJs), also have diurnal variations (Du et al., 2015, 2022; Kong et al., 2020; Lima et al., 2022; Stensrud, 1996).

A notable diurnal phenomenon is the offshore propagation of rainfall and winds observed off coasts globally (Du & Rotunno, 2015; Fang & Du, 2022; Mapes et al., 2003; Peng & Chen, 2023; Yang & Slingo, 2001; Yang & Smith, 2006; Yokoi et al., 2017). Yang and Slingo (2001) identified strong diurnal signals spreading out from the land to sea in the Bay of Bengal, New Guinea and Mexico. Fang and Du (2022) found this offshore propagation primarily occurs at low latitudes, and is explained by inertia-gravity waves resulting from diurnally varying thermal contrast near tropical or subtropical coasts. This theoretical examination of this mechanism uses a linear theory of land and sea breezes (Drobinski et al., 2011; Jiang, 2012; Qian et al., 2009; Rotunno, 1983). The land-sea breezes manifest as either inertia-gravity waves at low latitude or trapped circulations at high latitude, determining whether diurnal signals propagate offshore or are in phase (Du & Rotunno, 2015). Background winds can also impact offshore propagation by changing inertia-gravity wave patterns (Du & Rotunno, 2018).

In the South Asian monsoon region, satellite observations in the Bay of Bengal have revealed the offshore co-propagation of winds and diurnal rainfall signals from the east coast of India into the Bay of Bengal at a speed of around 18 m s^{-1}, and the maximum convergence of surface wind precedes the maximum rainfall by 1–2 hr, indicating the presence of inertia-gravity waves driven by diurnal thermal contrast between Indian subcontinent

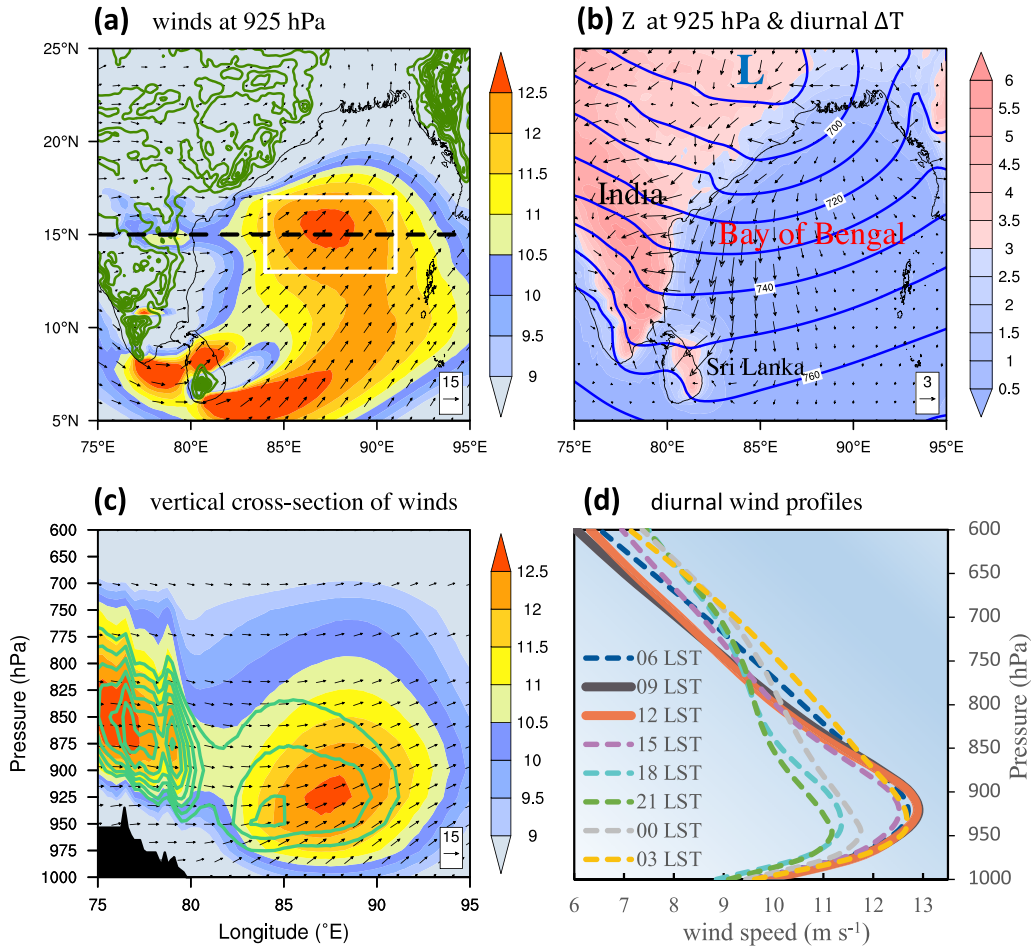

Figure 1. Horizontal and vertical structure of monsoon LLJ and its diurnal variation. (a) Horizontal distribution of daily mean wind speed (color shaded, m s^{-1}) and wind vectors at 925 hPa. The green contours indicate the terrain greater than 200 m with a 200 m interval. (b) The differences in temperature below 925 hPa (K) and winds at 925 hPa (black vectors) between daytime (16 local standard time (LST)) and nighttime (04 LST), superimposed with the geopotential height at 925 hPa (blue contours, gpm). (c) Vertical cross-section of daily mean wind speed (shaded, m s^{-1}) and horizontal wind vectors along the black dashed line in (a). The green contours (greater than 12 m s^{-1} in a 0.5 m s^{-1} interval) represent the wind speeds at 03 LST. The terrain is indicated by black shading. (d) Diurnal evolution of vertical wind profiles (m s^{-1}) averaged over the white box in (a).

and the Bay of Bengal (Kilpatrick et al., 2017). Li and Carbone (2015) found that mid-tropospheric westerlies facilitate eastward propagation from India but hinder westward propagation from Burma because strong onshore winds make the inertia-gravity wave dissipate owing to Doppler effect.

During the summer, the Bay of Bengal experiences low-level monsoon flows that come from India and turn northeastward (Fujinami et al., 2020, 2022), forming a strong southwesterly coastal LLJ (Figure 1a). Previous studies have documented that the LLJs over the Indian subcontinent exhibit a pronounced diurnal cycle with a nocturnal maximum, due to reduced frictional force and inertia oscillation of the winds (Blackadar, 1957; Chen, 2020). However, the control mechanism of diurnal variation of the marine LLJ over the Bay of Bengal remain unclear. This study hypothesizes that diurnal heating over India may influence the coastal LLJ via inertia-gravity waves, and the core location of the coastal LLJ may be modulated on the diurnal scale by such waves. This study aims to address the yet-to-be-documented question of whether the diurnal migration of LLJ over the Bay of Bengal exists and what factors affect this migration.

2. Data and Methods

2.1. Data

The fifth generation of the European Centre for Medium-Range Forecasts (ECMWF) global climate atmospheric reanalysis, ERA5, is employed to examine the diurnal variability of the monsoon LLJ and its associated atmospheric processes. The high spatial and temporal resolution of ERA5, with a horizontal grid spacing of $0.25° \times 0.25°$ and a time interval of 1 hr, makes it a widely used tool for detecting LLJs (Chen et al., 2021; Du & Chen, 2019; Lima et al., 2022; Luo & Du, 2023). The ERA5 data is averaged over the summer months of June-August for the years 1979–2018 to generate hourly mean climatologies. This approach allowed us specifically target the diurnal components.

2.2. Identification of the LLJ

The presence of LLJs is identified using two criteria: (a) a wind maximum exceeding 10 m s^{-1} below 700 hPa, and (b) a substantial vertical wind shear defined as a reduction in wind speed of over 3 m s^{-1} from the wind speed maximum upward to the subsequent wind speed minimum at or below the 600 hPa (Du & Chen, 2019; Whiteman et al., 1997).

2.3. A Linear Land-Sea Breeze Model

The linear equations of motion in two dimensions, incorporating a background wind and friction, can be described under the Boussinesq and hydrostatic approximation:

$$\left(\frac{\partial}{\partial t} + U\frac{\partial}{\partial x}\right)u - fv = -\frac{\partial \phi}{\partial x} - \alpha u \tag{1}$$

$$\left(\frac{\partial}{\partial t} + U\frac{\partial}{\partial x}\right)v + fu = -\alpha v \tag{2}$$

$$-b = -\frac{\partial \phi}{\partial z} \tag{3}$$

$$\left(\frac{\partial}{\partial t} + U\frac{\partial}{\partial x}\right)b + N^2 w = Q - \alpha b \tag{4}$$

$$\frac{\partial u}{\partial x} + \frac{\partial w}{\partial z} = 0. \tag{5}$$

Here, the variables u,v,w represent the wind components in the x, y, and z directions, respectively, U is a constant zonal background wind, ϕ is the geopotential, N is the Brunt-väisälä frequency, f is the Coriolis parameter, b is the buoyancy and the friction force is represented by (αu,αv) with a linear frictional coefficient α. The heating function is specified as $Q = Q_0\left[(\pi/2) - \arctan(x/x_0)\right]e^{-z/z_0}e^{-i\omega t}$, with x_0 and z_0 being the horizontal and vertical scale of heating, respectively, ω being 2π day^{-1}, and Q_0 representing the maximum heating rate at noon ($t = 0$) (Du & Rotunno, 2018; Rotunno, 1983). The coastline is located at $x = 0$ and separates land to the west and ocean to the east.

Equations 1–5 are combined into a single equation for the streamfunction ψ with $u = \frac{\partial \psi}{\partial z}$ and $w = -\frac{\partial \psi}{\partial x}$, resulting in

$$\left[f^2 + \left(\frac{\partial}{\partial t} + U\frac{\partial}{\partial x} + \alpha\right)^2\right]\frac{\partial^2 \psi}{\partial z^2} + N^2\frac{\partial^2 \psi}{\partial x^2} = -\frac{\partial Q}{\partial x}. \tag{6}$$

By assuming that $\psi = \mathrm{Re}(\Psi e^{-i\omega t})$, Equation 6 becomes

$$\left[f^2 + \left(-i\omega + U\frac{\partial}{\partial x} + \alpha\right)^2\right]\frac{\partial^2 \Psi}{\partial z^2} + N^2\frac{\partial^2 \Psi}{\partial x^2} = Q_0\left(\frac{x_0}{x_0^2 + x^2}\right)e^{-z/z_0} \tag{7}$$

The Fourier transform of Equation 7 in the x direction, $\hat{\psi} = \int_{-\infty}^{\infty} \Psi e^{-ikx}$ is given by:

$$\left(f^2 - \sigma^2\right)\frac{\partial^2 \hat{\psi}}{\partial z^2} - N^2 k^2 \hat{\psi} = \sqrt{\frac{\pi}{2}} Q_0 e^{-x_0|k|} e^{-z/z_0}, \tag{8}$$

where $\sigma = \omega - kU + i\alpha$. With the constraints of lower boundary condition $\hat{\psi} = 0$ at $z = 0$ and upper boundary condition $\hat{\psi}$ finite and satisfying the radiation condition when $z = \infty$, the solution of Equation 8 is given by

$$\hat{\psi} = \sqrt{\frac{\pi}{2}} \frac{Q_0}{\left[\frac{\left(f^2-\sigma^2\right)}{z_0^2}\right] - N^2 k^2} e^{-x_0|k|} \left(e^{-z/z_0} - e^{-\sqrt{N^2/\left(f^2-\sigma^2\right)}\, sng(k) kz}\right). \tag{9}$$

By utilizing the inverse Fourier transform, we obtain

$$\psi = \mathrm{Re}\left[\frac{1}{2\pi}\int_{-\infty}^{\infty} \hat{\psi} e^{i(kx-\omega t)} dk\right], \tag{10}$$

$$u = \frac{\partial \psi}{\partial z} = \mathrm{Re}\left[\frac{1}{2\pi}\int_{-\infty}^{\infty} \frac{\partial \hat{\psi}}{\partial z} e^{i(kx-\omega t)} dk\right], \text{and} \tag{11}$$

$$v = \mathrm{Re}\left[\frac{f}{i\omega - ikU - \alpha}\frac{1}{2\pi}\int_{-\infty}^{\infty} \frac{\partial \hat{\psi}}{\partial z} e^{i(kx-\omega t)} dk\right]. \tag{12}$$

In accordance with Du and Rotunno (2015, 2018), we set $f = 3.77 \times 10^{-5}\ \mathrm{s}^{-1}$ at 15°N, $\alpha = 0.2\omega$, $Q_0 = 1 \times 10^{-5} \mathrm{m\,s}^{-3}$, $z_0 = 1.5$ km, $x_0 = 50$ km, $N = 0.01\ \mathrm{s}^{-1}$ in solution of Equations 10 and 11. The numerical calculations for ψ, u, and v were performed using MATLAB.

3. Results

3.1. Diurnal Variation of the Monsoon Low-Level Jet

During the summer, strong southwesterly low-level winds occur over the Bay of Bengal, with a core centered approximately 15°N, 87°E (Figure 1a) and a maximum intensity at 925 hPa (Figure 1c). These winds meet the criteria for a LLJ (Du & Chen, 2019), as the wind maximum (~12.5 m s^{-1}) exceeds the 10 m s^{-1} below 700 hPa, and the wind speed decreases by 6.5 m s^{-1} below 600 hPa. The LLJ is formed by the confluence of two monsoon flows from the west (westerlies over India subcontinent) and south (southwesterlies surrounding the south of India). A low-pressure vortex can be observed at 925 hPa over the northeastern region of India (indicated by "L" in Figure 1b), causing southwesterly winds to prevail on the southeastern side of the vortex.

An evident diurnal variation of the monsoon LLJ in the center of Bay of Bengal is observed, with a morning maximum between 09 and 12 local standard time (LST) (Figure 1d). This contrasts with the nocturnal peak of LLJ over India or near its eastern coast reported in previous studies (Chen, 2020; Fujinami et al., 2021). The large differences between daytime and nocturnal winds occur near the eastern coastal region of India under the effect of diurnal land-sea thermal contrast (Figure 1b). At night (03 LST), the core of monsoon LLJ shifts closer to the coast rather than the center of the Bay of Bengal (Figure 1c). These results suggest that the locations of monsoon LLJ varies on a diurnal basis, which will be further investigated in the following section.

3.2. Offshore Migration of the Monsoon Low-Level Jet

Figure 2 illustrates the diurnal variation of horizontal winds at 925 hPa, showing the monsoon LLJ migrates offshore by approximately 600 km on a diurnal scale. Specifically, the jet core is typically located near the eastern coast of India (82–85°E) At 03 LS, gradually moving offshore to 87°E and becoming slightly stronger between 09 and 12 LST. By 18 LST, the jet core reaches the center of Bay of Bengal (90°E), but it weakens. The strength further decreases with the nearly stationary jet core from 18 LST to 00 LST. At 00 LST, another jet core begins to form near the coast (81°E) and repeats its diurnal offshore migration later.

The diurnal perturbation winds, depicted by black vectors in Figure 2, are obtained are calculated by taking the differences between the wind speeds and directions at each specific time of the day and the average (mean)

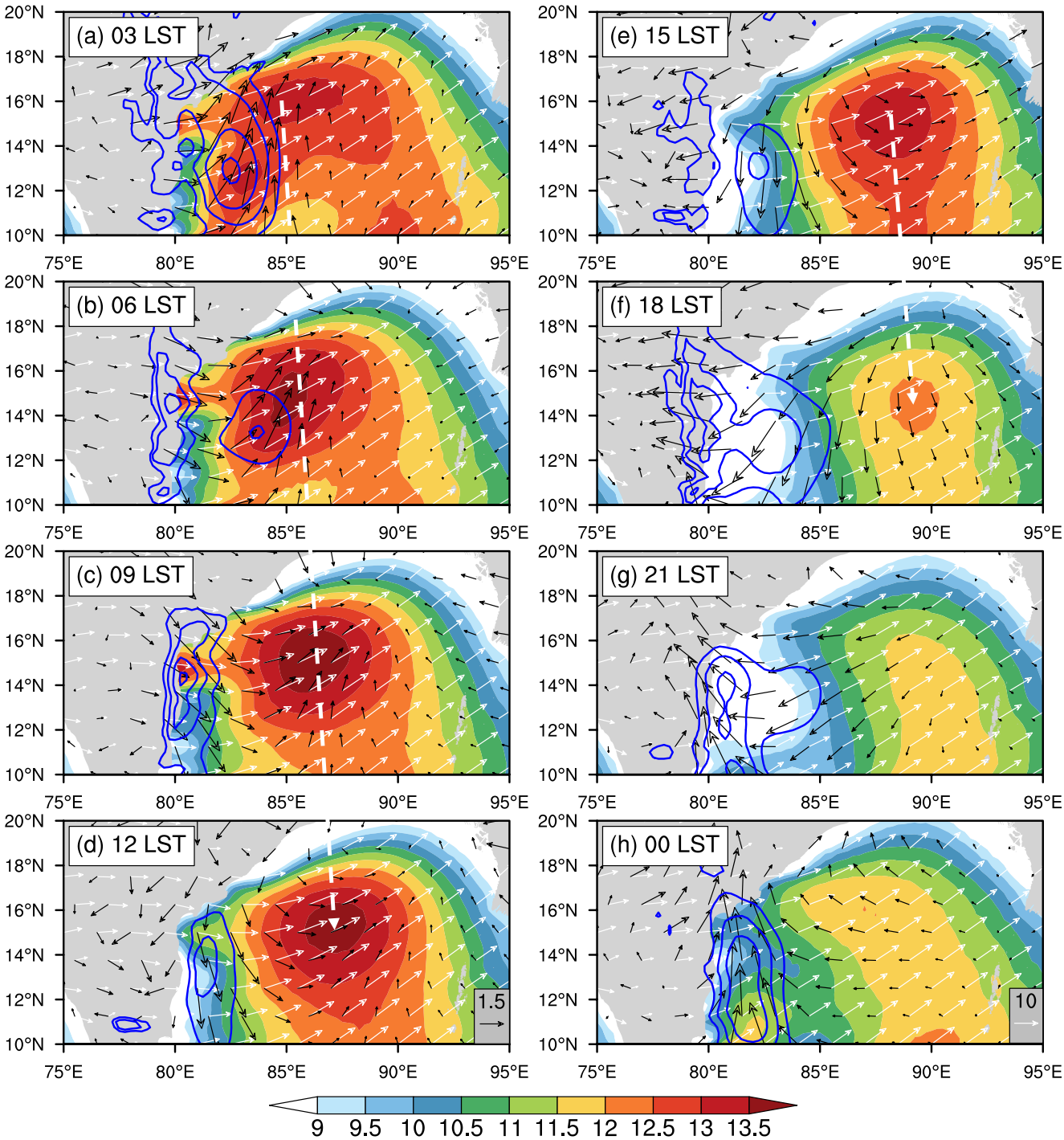

Figure 2. Diurnal offshore migration of monsoon LLJ and associated with diurnal wind perturbations. Diurnal evolution of wind speed (color shaded, m s^{-1}) and wind vectors (white) at 925 hPa, and diurnal wind deviation speed (blue contours greater than 2 m s^{-1} with intervals of 0.5 m s^{-1}) and wind deviation vectors (black) at 925 hPa. The thick white dashed arrows depict the diurnal offshore migration of the LLJ over the Bay of Bengal.

wind speeds and directions observed over the entire day. Notably, significant diurnal perturbation winds with magnitudes of approximately 3 m s^{-1} are observed near the eastern coast of India, as indicated by blue contours in Figure 2. These winds exhibit a clockwise rotation. At 18 LST, the perturbation winds are onshore, or easterly, and correspond to the sea breeze (Figure 2f). Conversely, at 06 LST, the winds are offshore, or westerly, and correspond to the land breeze (Figure 2b). This suggests that the perturbation winds are driven by the diurnal

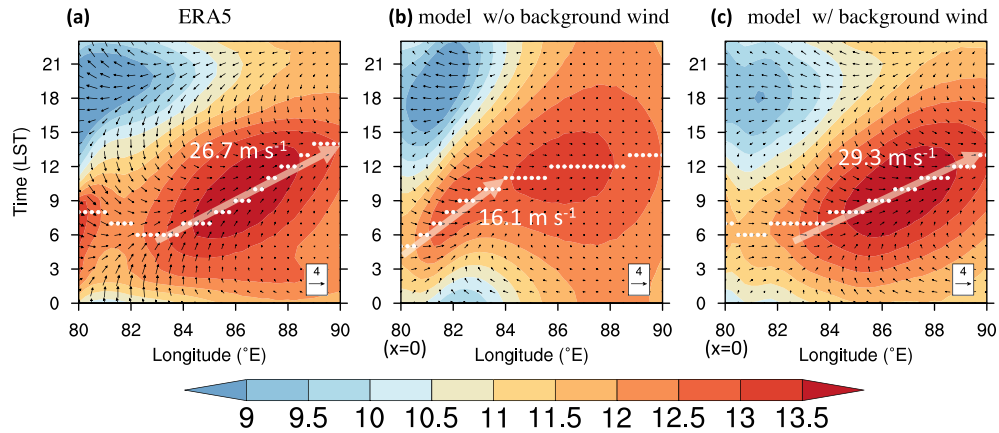

Figure 3. Comparisons in diurnal offshore migration of monsoon LLJ between ERA5 and analytical model. Longitude-time Hovmöller diagrams showing wind speed (color shaded, m s^{-1}) and perturbation horizontal wind vectors at 925 hPa along 15°N derived from (a) ERA5 analysis, (b) an analytical model without background wind, and (c) an analytical model with background wind. White dots indicate the diurnal wind peaks and white arrows are linearly regression of those peaks, indicating the offshore migration speed of the LLJ.

thermal contrast between land and sea (Figure 1b). Figure 1b shows that the temperature differences between daytime and nighttime over the land (e.g., India) are more significant than the ocean (e.g., Bay of Bengal).

While the maximum diurnal wind deviations primarily occur along the coast (blue contours in Figure 2), it is important to note that the clockwise rotation of diurnal perturbation winds also occur farther offshore, albeit with weakened intensity. The phase of diurnal wind deviations lags behind with increasing offshore distance, as seen in the westerly perturbation winds at 88°E at 00 LST when the coastal perturbation winds turn southerly (Figure 2h). The decaying magnitude and phase delay of diurnal wind deviations with increasing distance from the shore implies the offshore propagation and dispersion of inertia-gravity waves caused by the diurnal land-sea thermal contrast (their Figure 7 in Du & Rotunno, 2015). The winds are enhanced when the diurnal perturbation winds turn roughly parallel to the daily mean winds, and the times at which this occurs vary based on the distance from the shore, leading to the offshore migration of the jet. Since the daily mean core of the southwesterly jet is located near the 87°E (Figure 1a), the diurnal wind deviations in that region tend to veer toward a southwesterly direction just before the noon (Figures 2c and 2d). The enhanced wind associated with this veering contribute to the diurnal maximum of the LLJ occurring before the noon (Figure 1d).

The Longitude-Time Hovmöller diagram of winds at 925 hPa along 15°N (Figure 3a) provides clear evidence of the offshore migration of the jet. The core of the jet moves from 83°E to 90°E between 5 and 14 LST, with a migration speed of approximately 26.7 m s^{-1}. The migration track in the Hovmöller diagram is generally in agreement with the track of the southwesterly perturbation winds.

We further investigated the impact of monsoon synoptic scale systems on diurnal characteristics of the jet, focusing on specific monsoon seasons with varying occurrences of low-pressure systems near the Bay of Bengal. Based on an hourly global track data set (Vishnu et al., 2020), we identified "active years" with occurrence hours greater than the 75th percentile and "inactive years" with occurrence hours less than the 25th percentile (Figure S1a in Supporting Information S1). Figures S1b and S1c in Supporting Information S1 revealed that both active and inactive years exhibited similar offshore propagation patterns. However, during active years, the jet had slightly higher intensities and faster propagation speeds, likely due to slightly stronger zonal background winds.

Finally, the presence of gravity wave driven by the diurnal land-sea thermal contrast is further confirmed through diurnal analysis of the vertical cross-section of divergence and perturbation temperature perpendicular to the coasts (Figure 4). In the ocean, constant phase lines of temperature and divergence exhibit positive slopes ranging from 0.003 to 0.006, moving eastward and downward. These slopes align with the calculated slope derived from the dispersion relationship for hydrostatic inertia-gravity waves, represented by the equation $\frac{\sqrt{\omega^2-f^2}}{N} = 0.005$. The observed negative divergence and positive temperature perturbations also exhibit an in-phase relationship in accordance with the polarization relationship of inertia-gravity waves (Figure 4). These results provide evidence

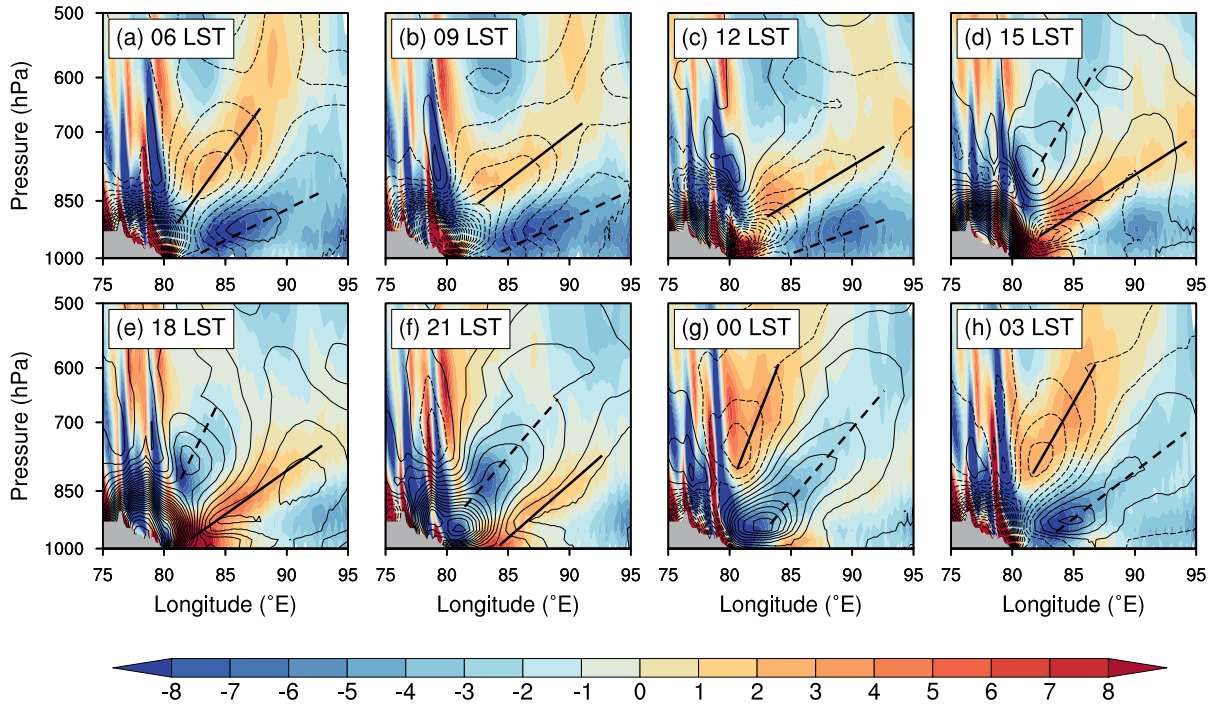

Figure 4. Diurnal evolution of inertia-gravity waves driven by diurnal land-sea thermal contrast. Vertical cross-section of divergence (color shaded, 10^{-6} s^{-1}) and perturbation temperature (contours with interval of 0.1 K, dashed contours indicate negative values) with diurnal variation. Black solid and dashed lines represent tilted phase rays of inertia-gravity waves.

for the existence of hydrostatic inertia-gravity waves. On the other hand, over the land, constant phase lines of temperature or divergence exhibit a westward tilt with height and are relatively stationary, suggesting mountain waves caused by the prevailing background westerlies.

3.3. Explanation From a Linear Land-Sea Breeze Model

We established a linear land-sea breeze model in two dimensions under the Boussinesq and hydrostatic approximation (see Section 2.3). This land-sea breeze model differentiates itself from previous works (e.g., Du & Rotunno, 2015, 2018; Qian et al., 2009; Rotunno, 1983), by incorporating both the background wind and friction.

In the absence of a background wind ($U = 0$), the streamfunction in the model takes the form of inertia-gravity waves that extend along ray paths extending upward and outward from the coast, similar to the findings of Du and Rotunno (2015) and is not shown here. The model's ability to replicate the diurnal fluctuations in the wind components near the coast is demonstrated through the Longitude-Time Hovmöller diagrams of u and v at 925 hPa (Figure 3b). However, the diurnal wind fluctuations are restricted to the coastal regions (80–83°E) rather than spreading further offshore. Furthermore, Figure 3b shows the full wind speeds, calculated by combining the simulated diurnal perturbation winds with the mean daily winds of ERA5 at 925 hPa along 15°N. The simulation highlights that the near-coastal jet can advance offshore but at a slower speed of approximately 16.1 m s^{-1}. On the other hand, the simulated jet in the center of the Bay of Bengal remains relatively stationary.

Considering the existence of actual westerlies with vertical wind shear below 400 hPa at the coast (15°N, 80°E, not shown), which is not accounted for in the linear model, we chose to use the observed mean wind over the lower tropospheric layer (approximately 6 m s^{-1} within 1,000–400 hPa) as a representative constant background wind in the linear model (Figure 3c). By adopting this approach, we successfully reproduced the diurnal perturbation winds nearshore and offshore, showing a close agreement with the corresponding winds from ERA5 (Figure 3a). As a result, the simulated jet is able to migrate significantly offshore with a comparable speed (29.3 m s^{-1}) and phase as ERA5 (26.7 m s^{-1}). This result highlights the importance of the presence of zonal background winds, which enables the inertial-gravity waves to have a more extensive downstream effect. The zonal background wind modulates the pattern of inertial gravity waves through Doppler shifting. The magnitude of this Doppler shifting

is directly correlated with the strength of the zonal background wind (U), with higher values of U resulting in greater tilting of the ray paths and a wider dispersion of wave energy (Du & Rotunno, 2018; Qian et al., 2009).

We conducted additional sensitivity experiments in the linear model, varying the zonal background winds ($U = 4$, 8, and 10 m s^{-1}) are performed. These experiments clearly demonstrate the presence of extensive downstream effect in all sensitivity experiments when compared to the baseline scenario with $U = 0$, although their diurnal propagation speeds were found to be sensitive (Figure S2 in Supporting Information S1). If we were to employ the zonal wind at a single layer (10 m s^{-1} at 925 hPa) as the constant background wind in the linear model, a significant discrepancy in the simulated diurnal propagation speed compared to ERA5. This emphasizes the need for further investigation into the effect of vertical wind shear in future studies.

Therefore, the linear land-sea breeze model that incorporates inertia-gravity waves driven by the diurnal land-sea thermal contrast can effectively capture the observed diurnal offshore migration of the LLJ, particularly when a westerly background wind is included in the model. The background wind enables the LLJ to migrate extensively offshore with a similar speed and phase as observed. To further examine the influence of westerly background winds, we conducted a comparison of the diurnal offshore migration of the LLJ before and after the onset of the Indian monsoon (May vs. June). These periods were selected due to significant differences in the intensity of the background zonal flows. In May (Figure S3a in Supporting Information S1) characterized by relatively weak zonal background winds (~0.4 m s^{-1}), the migration of LLJ is primarily confined near the coast, exhibiting a lower speed of 13.7 m s^{-1}. In contrast, in June (Figure S3b in Supporting Information S1), as the zonal background winds strengthen (~5.7 m s^{-1}), the LLJ exhibits an extended eastward migration with a higher speed of 23.4 m s^{-1}. This comparison provides further confirmation of the effect of westerly background winds on the behavior of the LLJ. Unlike the significant deviation before and after the monsoon onset, the intra-seasonal variation of the monsoon LLJ's diurnal offshore propagation is relatively small (Figures S3b–S3d in Supporting Information S1). However, we observed a slight increase in propagation speed from June to August (23.4 m s^{-1}, 24.4 m s^{-1}, and 25.4 m s^{-1}, respectively), attributed to a corresponding rise in background zonal flow (5.7 m s^{-1}, 6.9 m s^{-1}, and 7.5 m s^{-1}). This consistency supports our findings on the impact of zonal flow on the diurnal offshore propagation of the LLJ.

4. Conclusions

The present study provides a first examination of the diurnal migration of a southwesterly monsoon LLJ in the Bay of Bengal. The LLJ, which occurs during the summer months of June through August, and reaches its peak strength at 925 hPa, is found to exhibit a pronounced diurnal variation in both strength and location. Typically, the jet intensifies from midnight to morning, and weakens from noon to midnight, and shifts in location along the zonal direction. Figure 5 summarizes this process and associated mechanism.

The diurnal migration of LLJ starts near the eastern coast of India after midnight (Figure 5a), and gradually moves eastward toward the center of the Bay of Bengal until the afternoon (Figures 5b and 5c), with an offshore speed of approximately 26.7 m s^{-1}. This migration is caused by the varying phases of the clockwise rotation of diurnal perturbation winds in relation to offshore distance. Along the coast, significant onshore sea-breeze (offshore land-breeze) is observed in the late afternoon (early morning), while coast-parallel perturbation winds occur at noon or midnight. These veering perturbation winds extend offshore to the entire bay, though with weaker magnitude and a delayed phase. The delayed diurnal winds offshore are attributed to diurnal inertia-gravity waves caused by the land-sea thermal contrast at low latitudes. The presence of these waves is confirmed through analysis of dispersion and polarization relationships, with phase lines tilting eastward with height over the ocean, and the in-phase warm-temperature and convergence meeting the polarization relationship (Figure 5).

The study found that a linear land-sea breeze model that incorporates inertia-gravity waves driven by the diurnal land-sea thermal contrast can effectively capture the observed diurnal offshore migration of the LLJ, particularly when a westerly background wind is included in the model. The background wind enables the LLJ to migrate extensively offshore with a similar speed and phase as observed.

The significance of this study lies in its pioneering application of the theory of diurnal inertia-gravity waves to the diurnal migration of a jet, as previous studies have only applied this theory to the diurnal offshore propagation of rainfall (Fang & Du, 2022; Kilpatrick et al., 2017; Li & Carbone, 2015). Future research can explore the downstream impact of the offshore-moving LLJ on diurnal rainfall, as well as investigate the exist-

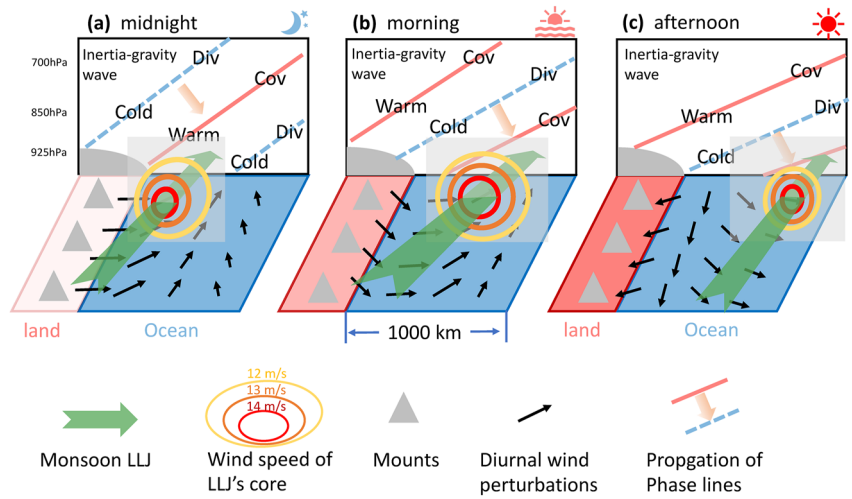

Figure 5. Conceptual model of the offshore migration of the monsoon LLJ driven by inertia-gravity waves resulting from the diurnal thermal contrast between land and sea. (a) At midnight, the southwesterly LLJ is located close to the coast because of diurnal southwesterly perturbations occurring offshore. (b) By morning, the LLJ migrates eastward and strengthens as southwesterly perturbations propagate eastward due to inertia gravity waves. (c) In the afternoon, the LLJ move further offshore but with a weakened intensity.

ence of similar migration phenomena in other coastal LLJs. It is important to note that there still exist some still discrepancy in the phase speed between the LLJ and precipitation, even when both are derived from ERA5. The mechanisms governing the diurnal propagation of rainfall are more complex than the migration of the LLJ alone. Factors such as cold pool dynamics (Jain et al., 2018) and convectively generated gravity waves (Love et al., 2011) can also influence the diurnal propagation of rainfall, in addition to gravity waves resulting from the land-sea thermal contrast. Given biases in ERA5 resulting from numerical resolution and convective parameterizations, it is imperative to utilize high-resolution simulations in order to gain a comprehensive understanding of the offshore propagation of rainfall and LLJ and their interactions. High-resolution model simulations, incorporating the analysis of vertical shear components, would be the most effective approach to address the complexities of the studied phenomena. Given the significant impact of topography on offshore propagation rainfall (Zhou et al., 2023), it would be intriguing to investigate the influence of topography in offshore LLJs through sensitivity experiments. The findings in the present study deepen our understanding of the complex dynamics of the southwesterly monsoon LLJ and provide a basis for future research on the regional monsoon system.

Data Availability Statement

The ERA5 reanalysis data used in this study are available from the Copernicus Climate Data Store at https://cds.climate.copernicus.eu/.

Acknowledgments
This study was supported by the Guangdong Major Project of Basic and Applied Basic Research (2020B0301030004), the National Natural Science Foundation of China (Grants 42075006 and 42122033), and the Key Innovation Team of China Meteorological Administration (CMA2023ZD08). The author is immensely grateful to the editor (Dr. Alessandra Giannini) and two anonymous reviewers for taking the time to review our paper and provide comprehensive comments.

References

Blackadar, A. K. (1957). Boundary layer wind maxima and their significance for the growth of nocturnal inversions. *Bulletin of the American Meteorological Society*, *38*(5), 283–290. https://doi.org/10.1175/1520-0477-38.5.283

Chen, G. (2020). Diurnal cycle of the Asian summer monsoon: Air pump of the second kind. *Journal of Climate*, *33*(5), 1747–1775. https://doi.org/10.1175/jcli-d-19-0210.1

Chen, G., Du, Y., & Wen, Z. (2021). Seasonal, interannual, and interdecadal variations of the East Asian summer monsoon: A diurnal-cycle perspective. *Journal of Climate*, *34*(11), 4403–4421. https://doi.org/10.1175/jcli-d-20-0882.1

Drobinski, P., Rotunno, R., & Dubos, T. (2011). Linear theory of the sea breeze in a thermal wind. *Quarterly Journal of the Royal Meteorological Society*, *137*(659), 1602–1609. https://doi.org/10.1002/qj.847

Du, Y., & Chen, G. (2019). Climatology of low-level jets and their impact on rainfall over southern China during the early-summer rainy season. *Journal of Climate*, *32*(24), 8813–8833. https://doi.org/10.1175/jcli-d-19-0306.1

Du, Y., Chen, Y. L., & Zhang, Q. (2015). Numerical simulations of the boundary layer jet off the southeastern coast of China. *Monthly Weather Review*, *143*(4), 1212–1231. https://doi.org/10.1175/mwr-d-14-00348.1

Du, Y., & Rotunno, R. (2015). Thermally driven diurnally periodic wind signals off the east coast of China. *Journal of the Atmospheric Sciences*, *72*(7), 2806–2821. https://doi.org/10.1175/jas-d-14-0339.1

Du, Y., & Rotunno, R. (2018). Diurnal cycle of rainfall and winds near the south coast of China. *Journal of the Atmospheric Sciences*, *75*(6), 2065–2082. https://doi.org/10.1175/jas-d-17-0397.1

Du, Y., Shen, Y., & Chen, G. (2022). Influence of coastal marine boundary layer jets on rainfall in South China. *Advances in Atmospheric Sciences*, *39*(5), 782–801. https://doi.org/10.1007/s00376-021-1195-7

Fang, J., & Du, Y. (2022). A global survey of diurnal offshore propagation of rainfall. *Nature Communications*, *13*(1), 7437. https://doi.org/10.1038/s41467-022-34842-0

Fujinami, H., Fujita, K., Takahashi, N., Sato, T., Kanamori, H., Sunako, S., & Kayastha, R. B. (2021). Twice-daily monsoon precipitation maxima in the Himalayas driven by land surface effects. *Journal of Geophysical Research: Atmospheres*, *126*(13), e2020JD034255. https://doi.org/10.1029/2020jd034255

Fujinami, H., Hirata, H., Kato, M., & Tsuboki, K. (2020). Mesoscale precipitation systems and their role in the rapid development of a monsoon depression over the Bay of Bengal. *Quarterly Journal of the Royal Meteorological Society*, *146*(726), 267–283. https://doi.org/10.1002/qj.3672

Fujinami, H., Sato, T., Kanamori, H., & Kato, M. (2022). Nocturnal southerly moist surge parallel to the coastline over the western Bay of Bengal. *Geophysical Research Letters*, *49*(18), e2022GL100174. https://doi.org/10.1029/2022gl100174

Jain, D., Chakraborty, A., & Nanjundaiah, R. S. (2018). A mechanism for the southward propagation of mesoscale convective systems over the Bay of Bengal. *Journal of Geophysical Research: Atmospheres*, *123*(8), 3893–3913. https://doi.org/10.1002/2017jd027470

Jiang, Q. (2012). On offshore propagating diurnal waves. *Journal of the Atmospheric Sciences*, *69*(5), 1562–1581. https://doi.org/10.1175/jas-d-11-0220.1

Johnson, R. H. (2011). Diurnal cycle of monsoon convection. In *The global monsoon system: Research and forecast* (pp. 257–276).

Kilpatrick, T., Xie, S. P., & Nasuno, T. (2017). Diurnal convection-wind coupling in the Bay of Bengal. *Journal of Geophysical Research: Atmospheres*, *122*(18), 9705–9720. https://doi.org/10.1002/2017jd027271

Kong, H., Zhang, Q., Du, Y., & Zhang, F. (2020). Characteristics of coastal low-level jets over Beibu Gulf, China, during the early warm season. *Journal of Geophysical Research: Atmospheres*, *125*(14), e2019JD031918. https://doi.org/10.1029/2019jd031918

Li, Y., & Carbone, R. E. (2015). Offshore propagation of coastal precipitation. *Journal of the Atmospheric Sciences*, *72*(12), 4553–4568. https://doi.org/10.1175/jas-d-15-0104.1

Lima, D. C., Soares, P. M., Nogueira, M., & Semedo, A. (2022). Global coastal low-level wind jets revisited through the new ERA5 reanalysis. *International Journal of Climatology*, *42*(9), 4491–4507. https://doi.org/10.1002/joc.7482

Love, B. S., Matthews, A. J., & Lister, G. M. S. (2011). The diurnal cycle of precipitation over the Maritime Continent in a high-resolution atmospheric model. *Quarterly Journal of the Royal Meteorological Society*, *137*(657), 934–947. https://doi.org/10.1002/qj.809

Luo, Y., & Du, Y. (2023). The roles of low-level jets in "21·7" Henan extremely persistent heavy rainfall event. *Advances in Atmospheric Sciences*, *40*(3), 350–373. https://doi.org/10.1007/s00376-022-2026-1

Mapes, B. E., Warner, T. T., & Xu, M. (2003). Diurnal patterns of rainfall in northwestern South America. Part III: Diurnal gravity waves and nocturnal convection offshore. *Monthly Weather Review*, *131*(5), 830–844. https://doi.org/10.1175/1520-0493(2003)131<0830:dporin>2.0.co;2

Peng, C.-H., & Chen, X. (2023). Warm-season afternoon precipitation peak in the central Bay of Bengal: Process-oriented diagnostics. *Journal of Geophysical Research: Atmospheres*, *128*(13), e2022JD038398. https://doi.org/10.1029/2022jd038398

Qian, T., Epifanio, C. C., & Zhang, F. (2009). Linear theory calculations for the sea breeze in a background wind: The equatorial case. *Journal of the Atmospheric Sciences*, *66*(6), 1749–1763. https://doi.org/10.1175/2008jas2851.1

Rotunno, R. (1983). On the linear theory of the land and sea breeze. *Journal of the Atmospheric Sciences*, *40*(8), 1999–2009. https://doi.org/10.1175/1520-0469(1983)040<1999:otltot>2.0.co;2

Stensrud, D. J. (1996). Importance of low-level jets to climate: A review. *Journal of Climate*, *9*(8), 1698–1711. https://doi.org/10.1175/1520-0442(1996)009<1698:iolljt>2.0.co;2

Vishnu, S., Boos, W. R., Ullrich, P. A., & O'Brien, T. A. (2020). Global track dataset of monsoon low pressure systems [Dataset]. Zenodo. https://doi.org/10.5281/zenodo.3890646

Whiteman, C. D., Bian, X., & Zhong, S. (1997). Low-level jet climatology from enhanced rawinsonde observations at a site in the southern Great Plains. *Journal of Applied Meteorology*, *36*(10), 1363–1376. https://doi.org/10.1175/1520-0450(1997)036<1363:lljcfe>2.0.co;2

Yang, G., & Slingo, J. (2001). The diurnal cycle in the tropics. *Monthly Weather Review*, *129*(4), 784–801. https://doi.org/10.1175/1520-0493(2001)129,0784:TDCITT.2.0.CO;2

Yang, S., & Smith, E. A. (2006). Mechanisms for diurnal variability of global tropical rainfall observed from TRMM. *Journal of Climate*, *19*(20), 5190–5226. https://doi.org/10.1175/jcli3883.1

Yokoi, S., Mori, S., Katsumata, M., Geng, B., Yasunaga, K., Syamsudin, F., & Nurhayati, Y. K. (2017). Diurnal cycle of precipitation observed in the western coastal area of Sumatra Island: Offshore preconditioning by gravity waves. *Monthly Weather Review*, *145*(9), 3745–3761. https://doi.org/10.1175/mwr-d-16-0468.1

Zhou, Y., Wang, S., & Fang, J. (2023). Diurnal cycle and dipolar pattern of precipitation over Borneo during the MJO: Linear theory and nonlinear sensitivity experiments. *Journal of Geophysical Research: Atmospheres*, *128*(5), e2022JD037616. https://doi.org/10.1029/2022jd037616